Journal Pre-proofs

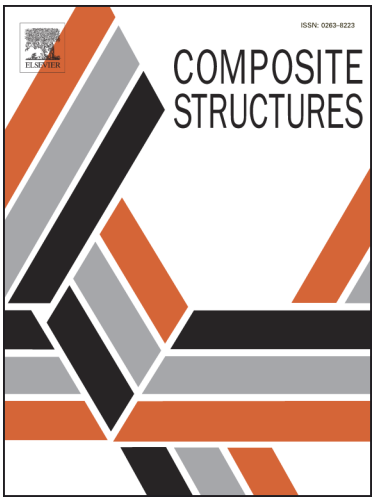

Shear Driven Deformation and Damage Mechanisms in High-performance Carbon Fibre-reinforced Thermoplastic and Toughened Thermoset Composites Subjected to High Strain Loading

Thibault. P. A. Hernandez, Andrew R. Mills, Hamed Yazdani Nezhad

PII: S0263-8223(20)33215-3
DOI: https://doi.org/10.1016/j.compstruct.2020.113289
Reference: COST 113289

To appear in: *Composite Structures*

Received Date: 14 May 2020
Revised Date: 19 August 2020
Accepted Date: 1 November 2020

Please cite this article as: P. A. Hernandez, Thibault., Mills, A.R., Yazdani Nezhad, H., Shear Driven Deformation and Damage Mechanisms in High-performance Carbon Fibre-reinforced Thermoplastic and Toughened Thermoset Composites Subjected to High Strain Loading, *Composite Structures* (2020), doi: https://doi.org/10.1016/j.compstruct.2020.113289

Shear Driven Deformation and Damage Mechanisms in High-performance Carbon Fibre-reinforced Thermoplastic and Toughened Thermoset Composites Subjected to High Strain Loading

Thibault. P. A. Hernandez[1], Andrew R. Mills[1,*] and Hamed Yazdani Nezhad[2,**]

[1]Enhanced Composite & Structures Centre, School of Aerospace, Transport and Manufacturing, Cranfield University, UK

[2]Aerospace Research Centre, Department of Mechanical Engineering and Aeronautics, City, University of London, UK

Corresponding authors: *A.R.Mills@cranfield.ac.uk and **hamed.yazdani@city.ac.uk

Keywords: CFRP composite; PEEK; Shear damage; Plasticity; High strain; Fibre-matrix debonding

Abstract

High strain loading response of high-performance aerospace grade polyether-ether-ketone (PEEK) and toughened epoxy carbon fibre-reinforced composites has been investigated in pre-impregnated laminates having identical carbon fibre volume fraction, i.e. nearly 65%. Tensile cyclic loading tests have been carried out on the laminates with $[\pm 45^\circ]_{8S}$ stacking sequence, in order to characterise inelastic (plasticity) parameters for the two laminates progressively up to high strains (up to 11% strains), in correlation with the fibre and matrix micro-scale deformation and damage characteristics. The most suitable processes to achieve ultimate mechanical performance were used for manufacturing of the laminates. It has been observed that the PEEK composite exhibits higher mechanical performance at high strains under cyclic loads compared to epoxy composites (150% ultimate failure strain, 380% strain hardening and 200% ultimate failure stress) due to having superior micro-scale shear deformation in PEEK attributed to interfacial strength of fibre-matrix prior to the ultimate failure, as opposed to extensive micro-cracking, coalescence and fibre-matrix debonding in the epoxy composite.

1. Introduction

High performance structures (e.g. aerospace, automotive and energy components) are transitioning from conventional materials to new advanced materials particularly made of carbon fibre-reinforced polymer (CFRP) composites having high carbon fibre

content (e.g. > 60% volume fraction). This transition is directly linked with the need for lightness and performance efficient structures in terms of lifetime, maintenance levels and structural integrity. Among the CFRP composites, those with epoxy polymer matrix have low strain energy absorbance behavior when are subjected to impact or relatively high strains. Such composites develop cracks extensively in the matrix, at the plies interface (e.g. interlaminar delamination), and at the fibre-matrix interface, mainly resulting from the brittleness of the thermoset polymer bonds at failure [1, 2]. Toughened resin systems have, thus, been introduced such as introduction of rubber or polymeric nanoparticles in M21 or 977-6 epoxy matrices [3], and/or use of thermoplastic, particularly polyether-ether-ketone (PEEK) as matrix (having a high glass transition temperature and low moisture absorbance [4]). Increase in toughness leads to high mechanical performance due to allowing for dissipation of strain energy via microstructural deformation mechanisms rather than damage [5-8]. Moreover, it leads to high energy impact resistance, high damage growth resistance, and resilience and reliability after damage or notches.

Since the introduction of thermoplastic materials in high-performance structures in the 1980's [9], the quality of thermoplastic CFRP composite materials has significantly been improved [9-12]. Their high plasticity range and toughness ensures high reliability of thermoplastic structures, as also demonstrated in laboratory scale experiments in this study.

The present article investigates the evolution of damage and deformation in high toughness PEEK (TC1200/IM7) and epoxy 977-6 (977-6/T800) CFRP composites with approximately identical carbon fibre content (~65 Vol.%). Monolithic and cyclic tensile loading reaching near the ultimate failure points of the composites have been carried out to establish the differences in straining characteristics.

2. PEEK and Epoxy CFRP Composites Manufacturing

Two aerospace grades unidirectional (UD) CFRP pre-impregnated plies were selected: 1- a toughened epoxy matrix system (Cytec product 977-6/T800 [3]), and 2- a thermoplastic PEEK matrix (Toray Advanced Composites' product TC1200/IM7 [4]). The UD plies had identical layer thickness (nominal 140 microns) as well as identical carbon content in order to enable comparison of the mechanical performance. As-received supplied pre-preg CFRPs were processed for this study, therefore the carbon reinforcement type differed in the PEEK and epoxy specimens:

T800 exhibits 2% strain and 5.5GPa at failure, possessing the modulus of 300GPa, while the IM7 fibres exhibit similar failure strain to T800 but at a tensile strength of 3.0GPa and the modulus of 200GPa, therefore the T800 fibres alone possess superior properties in tension. It is noteworthy that the two materials selected for this study have been extensively used in aerospace applications, and as such the thermoset material is a toughened epoxy. In that sense, the authors would admit that its response must be different to that of an untoughened epoxy material. However it is emphasised that a selection of a toughened epoxy to compare with a high performance thermoplastic for this study would exhibit the optimal performance of such thermoset materials operating in high strain loaded applications (e.g. in wing structures) against the thermoplastic's response.

Both laminates were manually stacked with a $[+45/-45]_{8S}$ stacking sequence suitable for characterisation of the shear performance and inelastic parameters under cyclic loading [13-15]. Although some studies used an identical manufacturing process for both types [16, 17], their optimum manufacturing processes were significantly different, induced by different process parameters such as crystallinity in the thermoplastic laminates [17]. In order to ensure that the ultimate mechanical properties are reached, the laminates were manufactured using the most efficient recommended processes:

The epoxy system, 977-6/T800, is best processed using a vacuum bagging autoclave process which provides efficient laminate properties, as a standardised industrial process. The epoxy laminates' curing cycle was carried out according to the recommended specifications outlined in [3] with a temperature ramp rate of 2°C/min from room temperature to 135°C, a curing duration of three hours under uniform pressure of 6.9 Bar. The cooling phase used a rate of 3°C/min down to room temperature.

Even though the autoclave process was an option for the PEEK laminate, many studies have shown that PEEK laminates may suffer from reduction in interlaminar strength if processed at standard autoclave pressures [17, 18]. So, relatively higher pressure (> 7 bar) is recommended to provide sufficient consolidation. The compression moulding process for the PEEK laminates was selected to provide optimised integrated laminate. A matched face mould was designed for hot-press moulding process. D2 type steel was used for the mould due to its high hardness and low, stable thermal expansion coefficient at moulding temperature of 385°C

which is required for processing PEEK [4]. ±45° plies in dimension of 150mm×100mm were manually stacked into the mould cavity. The mould was then closed and heated up to 385°C under the pressure of 17 bar to ensure full wetting of carbon fibres and consolidation. The dwell at high temperature was 30 minutes in accordance to the material's specifications. Cooling was unforced air down to room temperature while maintaining the pressure, i.e. the PEEK laminate was ensured, firstly via the relatively high-pressure compression in a fixed D2-steel cavity, not to be exposed to air environment following industrially advised thermal cycle provided by Toray, secondly via cooling post process under the pressure (and not in air) with compression moulds not being lifted up, and thirdly via cutting laminate's edges off our study in case of possible effects from air tapping onto the edges of the material across the moulding, compression and cooling processes. Thereby, it was ensured that there was no or slight thermo-oxidative degradation of the PEEK matrix. A crystallinity level of approx. 35% was achieved post 1°C/min cooling rate. Both panel types were finely cut into smaller specimens, ensuring no damage introduction.
It may be noted that though substantial effects from process parameters on polymer composites have numerously been addressed in literature, the current article does not investigate such effects on the examined thermoplastic and thermoset materials. Instead, optimal, adopted industrial processes (thermoplastic pressed and thermoset autoclaved) have been selected to achieve the optimal materials' mechanical properties before conducting the tests. Therefore, the research does not examine process parameters' effects but stresses the high strain loaded applications (e.g. in highly deformed wing structures) pre-ensuring that the materials have reached their optimal mechanical properties. In that sense our research paves the way for understanding the behaviour of the two materials mainly via study of the trends of the stress-strain curves, shear and microscopic damage evolution.

3. High Strain Testing of Composite Laminates

The TP and TS laminates were inspected visually post process, using non-destructive thermography inspection and ultrasound C-scanning to ensure no process-induced defects (e.g. voids or disbond) prior to testing. The laminates were then cut to make 125mm×25mm tension specimens which were setup to be loaded in cyclic tension up to the ultimate failure strains (as examined monolithically, ~7% for the epoxy and ~11% for the PEEK composite) to allow nonlinear inelastic behaviour of the laminates. Moreover, the ±45° ply orientations allow quantification of fibre-matrix bond quality, and thus the shear damage in the laminates made by

different polymers. A calibrated and instrumented tensile test Instron facility equipped with load cell and displacement sensor (LVDT) was used for the tests. The tests were set to be load controlled to allow high strains reach at the ultimate failure point. Note that a laser extensometer was used to acquire real-time displacement in during testing.

The loading rate was set to be lower than 1 mm/min, sufficiently slow to ensure that a quasi-static result is obtained, according to [19], and to avoid interference of dynamic effects such as the strain rate dependence [20, 21].

The maximum total stress and strain in each laminate was obtained via study of the cyclic force-displacement (equivalent stress-strain) data. The data was studied along with the evolution of damage and deformation in the microstructure (using scanning electron microscopy, SEM, and optical microscopy) with respect to the increasing number of cycles. Minimum five cycles were required to obtain repeatable measurement of the evolution of microstructural damage and plasticity according to best practice recommendations [22, 23]. Selection of the interrupted cycles was based on preliminary monolithic loading of the laminates up to the failure point:

A maximum load value was selected close to the load at which the ultimate strength was reached in each laminate; the maximum load was then divided to five equal load steps, and was assigned to be the load of each cycle. The 4kN load level was decided to be the first cycle load for the two laminates in order to study the strain energy dissipation at the initial phase of straining (<0.5%). For the purpose of clamping specimens in the test machine, 25mm×50mm end tabs were adhered to all specimens using cyanoacrylate superglue, as shown in Figure 1.

Table 1 summarises the five cycles' load levels and their corresponding engineering stresses at which the tests were interrupted for cut-sectioning and microscopic investigations:

4. Correlation of Shear Strain and Damage Evolution

Cyclic testing of ±45° laminates relies upon a number of parameters in order to properly characterise the inelastic behaviour of the laminates during loading. A continuum damage mechanics approach based on the in-plane Ladeveze model [23, 24] has been taken for evaluation of damage parameters. It has been assumed that the shear strain and damage evolution is a function of shear modulus at each cycle and the evolution of thermodynamic shear forces. It is also assumed that the

interlaminar delamination is negligible (as also observed in our experiments) commonly observed in quasi-static cyclic loading scenario. Moreover for the ±45° laminates, the emphasis was made on the evaluation of shear damage (basically matrix shear and fibre-matrix debonding), and as such fibre breakage was not taken into account of damage evolution except at the ultimate failure which was driven by fibres' severe breakage (i.e. d_1).

The following sets of equations allow for quantification of stress-strain data and the shear modulus as schematically presented in Figure 2:

$$\begin{cases} \sigma_{12} = \sigma_x/2 \\ \gamma_{12} = \varepsilon_x - \varepsilon_y \\ \varepsilon_y = \nu\varepsilon_x \end{cases} \quad (1)$$

where σ_{12} and σ_x are shear stress and longitudinal stresses, respectively, γ_{12} is the in-plane shear strain, and ε_x and ε_y are normal strains in the longitudinal (0°) and transverse (90°) directions, respectively, correlated with the poison's ratio, ν.

The shear damage parameter defined in [22, 23] is calculated from the stress-strain data given in Eq. (1). The degradation of shear modulus, G_{12}^i, from its initial undamaged level (G_{12}^0) at cycle i (i=1 to 5) is therefore calculated from the stress-strain data at each cycle as per Figure 2. The shear damage parameter (d_{12}) is therefore given by [14]:

$$d_{12} = 1 - \frac{G_{12}}{G_{12}^0} \quad (2)$$

The d_{12} parameter is also a function of the mean value of the thermodynamic force, $\underline{Y_{12}}$ (analogous to strain energy release rates varying with the evolution of damage parameters), and is evaluated by [14]:

$$\underline{Y_{12}} = \sqrt{\frac{1}{2}G_{12}^0\gamma_{12}^2}\,, \quad (3)$$

at its initiation stage. Once the strain energy required to drive microstructural damage reaches a certain threshold, $\underline{Y_{12}^0}$, damage is initiated, and propagated at each cycle load until a maximum level of shear damage is reached (d_{max}), ideally equaling to the value of unity (1) in a pure shear mode. It is assumed that d_{12} is irreversible, meaning that its value does not become decrease at unloading in cyclic tests.

It is noteworthy that the actual ±45° specimens have been designed to evaluate the *shear* strain and damage parameters as a dominant mechanism, which is why the

evolution of matrix damage due to transverse loading (e.g. d_2) is not addressed in this study. However for $\gamma_{12} > 5\%$, as recommended by ASTM D3518, the ±45° specimen becomes invalid for accurate determination of shear performance due to fibres re-orientation. Therefore, careful consideration is accounted for in our discussion over the results in section 5.

5. Results and Discussion

5.1. Comparison of Stress-strain Data

The representative specimens post testing are shown in Figure 3, showing apparent elongated PEEK specimens at failure as opposed to slightly elongated epoxy laminates. It has also been observed that the PEEK specimens exhibited necking phenomenon at the middle of the length, initiated at the yield point and propagated with the increasing cycles to the whole length. The stress-strain raw data from the cyclic tests are shown in Figure 4(a). Four specimens per category were tested to ensure repeatability of the tests. The disparity between data for all tests was < 7%. Therefore, only one representative curve has been shown in Figure 4 in the interests of clear representation.

Data from both laminates show significant difference in the stress levels though the epoxy one shows, at the initial phase of small-scale deformations, slightly higher yield stress and tensile modulus attributed to the higher properties of the T800 fibres compared to the IM7 ones (described in section 2). A nonlinear trend is seen for the two laminates showing strain hardening behavior with the coefficients of 947 MPa and 250 MPa, respectively for the PEEK and epoxy laminates. The value of 947 MPa has been calculated at the blue mark on the PEEK curve which itself has been identified at a point at which the slope of the curve starts to grow though slightly. The slope is equal to (160.05 MPa – 143.01 MPa)/(0.101 – 0.083) = 946.67 MPa. Note that the value corresponds to the slope right before the blue mark, which has been almost stationary for a relatively large strain range.

The fibre re-orientation points were identified from Figure 4(a) data, at which a change in the stationary slope of the curves occurs, denoted by the blue marks in Figure 4(a). The blue marks have been transferred later on, to the curves in Figures 5 and 6 for further elaboration. The sudden change in the slope of the curves in Fig. 4(a) which has been stationary within a relatively wide range of strain variations, has

been the key to identify the re-orientation points for both laminates, though occurring slightly for the PEEK one.

Also, the point at which the rate of hardening increases is hindered in the PEEK by approximately 200% i.e. the occurrence is at much higher strain in the PEEK laminate compared to that in the epoxy one. The occurrence is linked with the dramatic deviation of the fibres from the ±45° direction towards the loading direction (i.e. 0° in Figure 1). In the PEEK laminate this is mitigated by the effect of necking, meaning that a slight increase in the hardening rate occurs (identified by blue points in the figure). However, the rate dramatically increases in the epoxy laminates due to lack of damage hindering given by the necking process as is in the PEEK ones. Such dramatic re-orientation in the epoxy laminate is attributed to extensive matrix damage and/or fibre-matrix debonding that results in reduction of transverse mechanical properties (observed herein and further discussed in section 5.3). Therefore, the straining performance of the PEEK matrix is higher by the order of 200%.

Figure 4(b) shows the magnified view of stress-strain data in the range between 0.0% and 1.2%. The laminates exhibit slight difference in the Young's modulus at the initial phase of the loading (first cycle), and almost an identical dissipated energy (area under the first hysteresis cycle loop). The area under the hysteresis loops at the subsequent cycles increases in the two laminates, a sign of growing dissipation of strain energy via deformation and damage.

For strains > 1% (Figure 4(c)), the strain hardening effect is considerably higher in the PEEK laminate. Higher contribution of shear deformation leading to the hardening rate of 947 MPa results from straining mechanism in the PEEK as opposed to the crack growth mechanisms (i.e. matrix micro-cracking and fibre-matrix debonding) in the epoxy one [25, 26]. Expectedly, the TP laminate shows a significantly higher strain near the ultimate failure point.

5.2. Comparison of Shear Damage Evolution

Shear modulus data (G_{12}) at each cycle was obtained from the slope of a straight line connecting the unloaded point on the γ_{12} axis, when σ_{12} tends to zero and the point at which the selected cycle stress ($2\sigma_{12}$) is reached, as shown schematically in Figure 2. The data are presented in Figure 5. Fibres re-orientation points have been identified via blue marks, corresponding to those identified in Figure 4. As seen, the

reduction in shear modulus follows an almost identical trend for the two laminates for σ < 150 MPa. The PEEK fails at much higher stress than the epoxy one. A sudden reduction in the epoxy composite's modulus occurs at $\sigma \simeq$ 150 MPa (at 3rd cycle's peak stress) as a result of extensive matrix cracking (microcrack coalescence discussed in the following section) followed by the dramatic fibre re-orientation (blue mark in Figure 4(a) for epoxy). Such reduction is recovered at σ > 170 MPa as the modulus increases due to fibres re-orientation towards loading direction. It is noteworthy that the definition of G_{12} may not be appropriate for such stress levels, to describe shear performance as fibres are not anymore in ±45° direction. ASTM D3518 has recommended a limit of 5% strain for such specimens to be valid for shear performance evaluation, thus the validity of G_{12} for σ > 170 MPa and $\gamma_{12} > 0.04$ is questioned since re-orientations have occurred beyond the 5% strain limit in the epoxy specimens. For the PEEK ones, G_{12} remains valid for definition of shear performance up to the blue marks at $\sigma \simeq$ 280 MPa. Nevertheless, the ultimate failure in the two laminates is fibre breakage.

Taking account of information provided in section 2, the T800 fibres possess higher properties than the IM7 ones, and one may conclude that this is in conflict with the stress-strain data presented where the epoxy laminate made of the T800 fibres fails earlier than the PEEK one made of the IM7. This is correct when the role of matrix properties in determination of the failure response is neglected. The data presented in Figures 4 and 5 clearly shows the significant contribution of PEEK matrix in mitigating such pre-mature failure (deformation apparent in Figure 3) whilst the epoxy matrix undergoing micro-cracking disrupt stress transfer across the laminate, and hands over the IM7 fibres a major fraction of load carrying capacity. In order to evaluate the contribution of shear damage parameter in the overall failure process, the following analysis has been provided:

Using equations (1-3), the value of d_{12} at each cycle has been calculated and presented in Figure 6 along with blue marks identified in it. As seen, damage in the epoxy laminate develops faster than that in the PEEK one by the order of > 200% at the initial stage of loading (1st cycle) where fibres are intact and slightly tensioned, which signs off a relatively significant contribution of epoxy damage as hypothesized above. Accounting for the validity up to the blue marks, the PEEK laminates reach the saturated shear damage of $d_{12} = 0.68$ and the epoxy ones, $d_{12} = 0.60$. Therefore,

the ultimate shear damage in epoxy laminates reaches a *saturation level* 13% higher than the PEEK ones prior to severe fibres re-orientation that later on leads to extensive damage in the epoxy matrix. Bearing in mind that the thermodynamic forces in the PEEK laminates, equivalent to matrix cracking induced strain energy release rates, have overperformed the epoxy ones by 120%.

Moreover, it is expected that beyond the blue marks at which $d_{12} >$ 0.60, fibre volume fractions dramatically increase (> 65%) and eventually fibre breakage becomes the dominant mechanism in determination of the ultimate failure of the composites. Such phenomenon is elaborated in the following paragraph:

At blue marks, it has been reasoned that severe fibre re-orientation process embarks on, posing large localised deformation. As a result, the matrix surrounding the severely re-oriented fibres is severely deformed until it experiences stresses beyond its ultimate strength, and is damaged failing to respond to high strain loading. Given no resistance arising from the damaged matrix material surrounding the fibres, the fibre re-orientation is boosted post blue marks (leading to increase in the slope), pushing back the damaged matrix and filling its space which leads to higher fibres volume fraction. Therefore, though the strain energy is dissipated via different mechanisms in the two laminates well before the re-orientation points, the ultimate failure solely depends on the fibres' performance.

5.3. Comparison of Microscopic Damage Evolution

The composite laminates were cut-sectioned from the lines identified in Figure 7. Fine diamond saw for composite cutting was initially utilised along with the use of non-reactive lubricant for avoiding cutting chips clustering. The cut samples were then cleaned off the lubricant, and smoothly polished using a standard polishing machine up to ultra-fine grain size (i.e. 4000 grade) so as to ensure a high quality cut surface without inducing damage as result of applying high machining and polishing loads. The microscopic observations were carried out using optical and SEM (using LYRA3 TESCAN) on the central region of the specimens (regions A and B identified in Figure 7). To enable such observations, a number of tests were interrupted at cycles 1, 3 and 5, and the laminates were cut post cycles. Figures 8 and 9 show the microscopic images for the PEEK and epoxy laminates, respectively. The values of shear strain, stress and damage parameters corresponding to the microscopic

images at cycles 1, 3 and 5 are tabulated in Table 2. Cycle 5 data have been labelled with asterisk symbols, identified as non-shear driven parameters as discussed for beyond-the-blue-marks validity in section 5.2.

No significant damage is observed at cycle 1 for the PEEK (Figure 8(a)) whilst slight matrix micro-cracks are seen for the epoxy laminate (Figure 9(a)). The prevailing mechanism is apparently linear elasticity in agreement with the phenomenological data presented for cycle 1 in Figure 4(b), with slight residual strain in the epoxy laminate.

Comparing cycle 3 images (Figure 8(b) and 9(b)), extensive matrix micro-cracking and fibre-matrix debonding in the epoxy laminate are observed as opposed to almost no-damage regions in the PEEK in Figure 9(b). This is identified as the distinct difference in shear damage and deformation mechanisms between the two matrix types at the early stage of straining (Cycle 3) before any severe re-orientation occurs when the both laminates are cycled up to > 50% of their ultimate strength (according to Table 1). The extensive development of matrix damage is seen in the two composites at cycle 5 (near-failure point) though in an instantaneously occurring cleavage fashion in the epoxy and a ductile bridging damage in the PEEK one. Moreover, the epoxy laminate exhibits extensive fibre-matrix debonding whilst almost none is observed in the PEEK one. It may be noted that the ultimate failure points identified in Table 1 are corresponding to fibre breakage dominantly occurring after extensive re-orientation (blue points identified in Figure 4(a)). Such extensive damage in the epoxy laminate is inclined with the remarks made in section 5.2 related to contribution of a follow-up fibre performance at the saturated damage level, i.e. loss of epoxy's load carrying capacity coupled with severe re-orientation.

Shear lines occurrence is also seen in Figure 8(c) at and after cycle 3. It is also seen that the PEEK matrix is deformed by shearing alongside and tangent to the carbon fibres, occurred near the re-orientation points. Such inelastic (residual) deformation mechanism has enabled the PEEK laminates to undergo a relatively high strain,

possessing lower d_{12}, and to fail at a significantly higher stress than the epoxy ones not bearing such residual shear lines (Figure 9(c)).

These observations in correlation with the macroscopic response (Figures 4-6), not only demonstrate the superior performance of the PEEK laminate before the severe re-orientation point and beyond that, also demonstrate superior ability for shear controlled deformation mechanisms near-failure point at high strains from which the smooth stress transfer would be further promoted at the interface of carbon fibres.

6. Conclusions:

Laboratory scale cyclic tests were carried out on the high-performance PEEK and epoxy composite laminates to characterise their mechanical performance at high strain levels (> 7% and 11% for epoxy and PEEK, respectively) under cyclic loads up to the ultimate failure point of the laminates. The tests were followed by microscopic investigations of deformation and damage mechanisms occurring in the matrices and at the interface with the fibres. Standard tensile test specimens with the $[\pm 45°]_{8S}$ stacking sequence were manufactured using the most suitable processes for manufacturing the two laminates to achieve their ultimate performance, in order for shear driven strain and damage to be quantified. Phenomenological major points on the stress-strain data were identified, evaluated and compared with respect to the micromechanical shear strain and damage mechanisms using optical and SEM microscopy.

It was shown that the PEEK laminate significantly outperforms the epoxy one in terms of maximum shear strain, ultimate failure stress and with a distinct strain hardening behavior (by the order of 150%, 200% and 380%, respectively) though it rivaled the epoxy laminate in terms of initial stiffness and yield strength.

The studies also showed a significantly faster shear damage evolution in the epoxy laminate, approximately double that in the PEEK one, driven by extensive matrix micro-cracking, followed by fibre-matrix debonding post cracks coalescence, supported by d_{12} calculations and the SEM images. The PEEK laminate, instead, exhibited a progressive shear strain and slight cracking at high strains as evident from the inelastic 30° shear lines within the matrix and at the interface tangent to the fibres, suggesting a material with superior shear performance at high strain operation, e.g. in a composite aircraft's wing undergoing large deformation.

Acknowledgments:

This study was supported by Safran Landing Systems, UK, and Toray Advanced Composites, Netherlands. This publication has also been partially supported by the UK Engineering and Physical Sciences Research Council funded research, STRAINcomp (Ref. EP/R016828/1). The underpinning data at DOI: 10.17862/cranfield.rd.12302153 can be accessed.

References:

[1] R. Talreja, "Fatigue of composite materials," (in English), *Modern Trends in Composite Laminates Mechanics,* Proceedings Paper no. 448, pp. 281-294, 2003.

[2] H. Y. Nezhad, F. Merwick, R. M. Frizzell, and C. T. McCarthy, "Numerical analysis of low-velocity rigid-body impact response of composite panels," (in English), *International Journal of Crashworthiness,* Article vol. 20, no. 1, pp. 27-43, Jan 2015, doi: 10.1080/13588265.2014.963378.

[3] *Cytec Technical Datasheet: Cycom 977-6 Epoxy Prepreg*, 2013. [Online]. Available: https://www.e-aircraftsupply.com/MSDS/10556CYCOM%20977-6%20tds.pdf.

[4] *Tencate Technical Datasheet: Cetex TC1200 PEEK Resin System*, 2014. [Online]. Available: https://www.tencatecomposites.com/product-explorer/products/ovl4/TenCate-Cetex-TC1200.

[5] H. Koerber, J. Xavier, P. P. Camanho, Y. E. Essa, and F. M. de la Escalera, "High strain rate behaviour of 5-harness-satin weave fabric carbon-epoxy composite under compression and combined compression-shear loading," (in English), *International Journal of Solids and Structures,* Article vol. 54, pp. 172-182, Feb 2015, doi: 10.1016/j.ijsolstr.2014.10.018.

[6] T. Hans and R. Hinterholzl, "A numerical approach modeling the braiding process for arbitrary mandrel shapes to calculate preform properties," presented at the 20th International Conference on Composite Materials, Copenhagen, Denmark, 2015.

[7] P. Morgan, *Carbon fibres and their composites*. CRC Press Taylor & Francis Group, 2005.

[8] Y. N. H and T. VJ, "Effect of morphological changes due to increasing carbon nanoparticles content on the quasi-static mechanical response of epoxy resin," *Polymers,* 2018 2018, doi: 10.3390/polym10101106.

[9] G. H. Melton, E. N. Peters, and R. K. Arisman, M. Kutz, Ed. *Applied Plastics Engineering Handbook, Chapter 2: Engineering Thermoplastics*, 1st Edition ed. Elsevier, 2011.

[10] A. Weber. (2018) Growing role of plastics in aerospace assembly. *Assembly*.

[11] A. G. Miller, D. T. Lovell, and J. C. Seferis, "THE EVOLUTION OF AN AEROSPACE MATERIAL - INFLUENCE OF DESIGN, MANUFACTURING AND IN-SERVICE PERFORMANCE," (in English), *Composite Structures,* Article vol. 27, no. 1-2, pp. 193-206, 1994, doi: 10.1016/0263-8223(94)90080-9.

[12] E. McHugh, D. Spagnuolo, A. Chin, E. Soc Plast, and E. Plast, "A COMPARISON OF A NEW WOVEN PEEK-CARBON FIBER COMPOSITE WITH APC-2 PREPREG," (in English), *In Search of Excellence /,* Proceedings Paper pp. 2008-2012, 1991.

[13] R. M. Frizzell, C. T. McCarthy, and M. A. McCarthy, "Simulating damage and delamination in fibre metal laminate joints using a three-dimensional damage model with cohesive elements and damage regularisation," (in English), *Composites Science and Technology,* Article vol. 71, no. 9, pp. 1225-1235, Jun 2011, doi: 10.1016/j.compscitech.2011.04.006.

[14] R. M. O'Higgins, C. T. McCarthy, and M. A. McCarthy, "Identification of Damage and Plasticity Parameters for Continuum Damage Mechanics Modelling of Carbon and

Glass Fibre-Reinforced Composite Materials," (in English), *Strain,* Article vol. 47, no. 1, pp. 105-115, Feb 2011, doi: 10.1111/j.1475-1305.2009.00649.x.

[15] R. M. O'Higgins, C. T. McCarthy, and M. A. McCarthy, "Effects of Shear-Transverse Coupling and Plasticity in the Formulation of an Elementary Ply Composites Damage Model, Part I: Model Formulation and Validation," *Strain,* vol. 48, no. 1, pp. 49-58, Feb 2012, doi: 10.1111/j.1475-1305.2010.00797.x.

[16] "Probabilistic Design Methodology for Composite Aircraft Structures - DOT/FAA/AR-99/2," 1999.

[17] Y. N. H, A. A, M. CT, and O. H. RM, "Impact damage response of carbon fibre-reinforced aerospace composite panels," 2015 2015, doi: 10.13140/RG.2.1.2174.4081. [Online]. Available: http://www.iccm-central.org/Proceedings/ICCM20proceedings/

[18] O. De Almeida, E. Bessard, and G. Bernhart, "Influence of processing parameters and semi-finished product on consolidation of carbon/peek laminates," presented at the 15th European Conference on Composite Materials, Venice, Italy, 2012.

[19] *ASTM D5961/D5961M, Standard Test Method for Bearing Response of Polymer Matrix Composite Laminates*, 1996.

[20] H. Koerber and P. P. Camanho, "High strain rate characterisation of unidirectional carbon-epoxy IM7-8552 in longitudinal compression," (in English), *Composites Part a-Applied Science and Manufacturing,* Article vol. 42, no. 5, pp. 462-470, May 2011, doi: 10.1016/j.compositesa.2011.01.002.

[21] H. Koerber, J. Xavier, and P. P. Camanho, "High strain rate characterisation of unidirectional carbon-epoxy IM7-8552 in transverse compression and in-plane shear using digital image correlation," (in English), *Mechanics of Materials,* Article vol. 42, no. 11, pp. 1004-1019, Nov 2010, doi: 10.1016/j.mechmat.2010.09.003.

[22] A. K. Pickett and M. R. C. Fouinneteau, "Material characterisation and calibration of a meso-mechanical damage model for braid reinforced composites," (in English), *Composites Part a-Applied Science and Manufacturing,* Article; Proceedings Paper vol. 37, no. 2, pp. 368-377, 2006, doi: 10.1016/j.compositesa.2005.03.034.

[23] P. Ladeveze and E. Ledantec, "DAMAGE MODELING OF THE ELEMENTARY PLY FOR LAMINATED COMPOSITES," *Composites Science and Technology,* vol. 43, no. 3, pp. 257-267, 1992, doi: 10.1016/0266-3538(92)90097-m.

[24] P. Ladeveze, "A DAMAGE COMPUTATIONAL METHOD FOR COMPOSITE STRUCTURES," (in English), *Computers & Structures,* Article; Proceedings Paper vol. 44, no. 1-2, pp. 79-87, Jul 1992, doi: 10.1016/0045-7949(92)90226-p.

[25] A. C. Garg and Y. W. Mai, "FAILURE MECHANISMS IN TOUGHENED EPOXY-RESINS - A REVIEW," (in English), *Composites Science and Technology,* Review vol. 31, no. 3, pp. 179-223, 1988, doi: 10.1016/0266-3538(88)90009-7.

[26] T. Kelly, B. M. Ghadi, S. Berg, and H. Ardebili, "In Situ Study of Strain-Dependent Ion Conductivity of Stretchable Polyethylene Oxide Electrolyte," (in English), *Scientific Reports,* Article vol. 6, p. 9, Feb 2016, Art no. 20128, doi: 10.1038/srep20128.

Tables:

Table 1: Cycles interrupted for microstructural investigation

Description	Epoxy CFRP	PEEK CFRP
Ultimate load in monolithic testing, kN	12.6	24.5
Selected maximum load, kN	12	20
1st cycle, kN (MPa)	4 (70)	4 (70)
2nd cycle, kN (MPa)	6 (105)	8 (140)
3rd cycle, kN (MPa)	8 (140)	12 (210)
4th cycle, kN (MPa)	10 (175)	16 (280)
5th cycle, kN (MPa)	12 (210)	20 (350)

Table 2: Comparison of γ_{12}, σ_{12} and d_{12} at cycles 1, 3 and 5 (near-failure points)

	PEEK laminate			Epoxy laminate		
	Cycle 1	Cycle 3	*Cycle 5	Cycle 1	Cycle 3	*Cycle 5
γ_{12}	0.24%	4.3%	*10.8%	0.3%	1.1%	*6.7%
σ_{12} (MPa)	35	105	*175	35	70	*105
d_{12}	0.45	0.60	*0.60	0.25	0.66	*0.6

Figures:

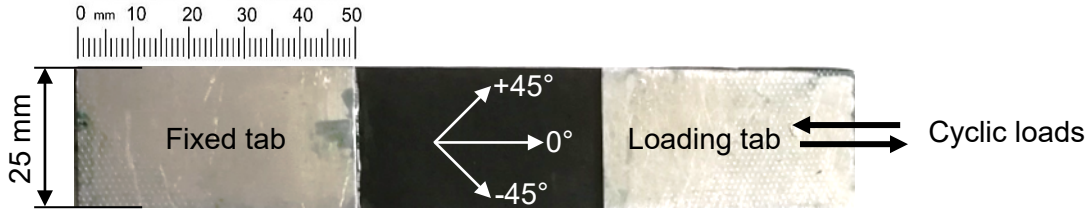

Figure 1. Tensile test specimen for monolithic and cyclic testing, with aluminum end tabs for clamping purpose

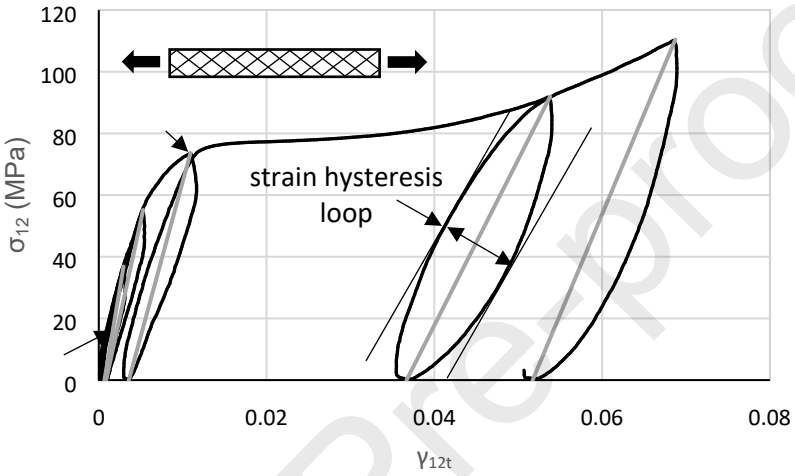

Figure 2. Typical stress-strain data for the ±45° CFRP laminates under tensile cyclic loads

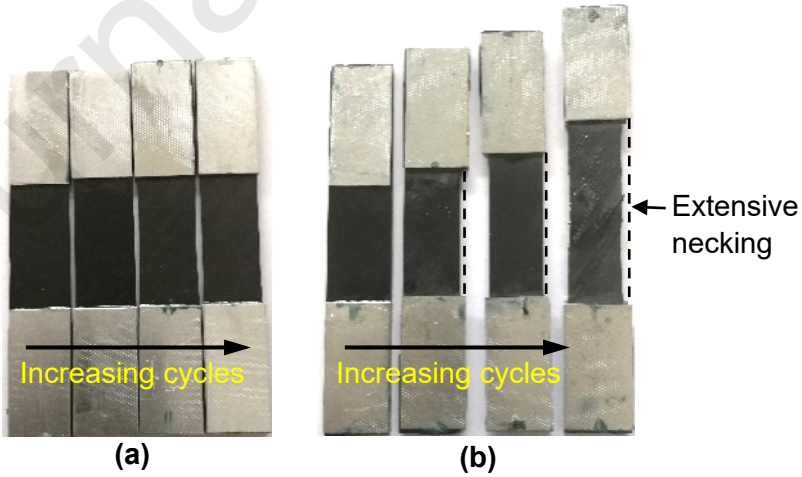

Figure 3. ±45° CFRP laminates (having width of 25 mm prior to loading) post cycles; (a) Epoxy laminates, (b) PEEK laminates

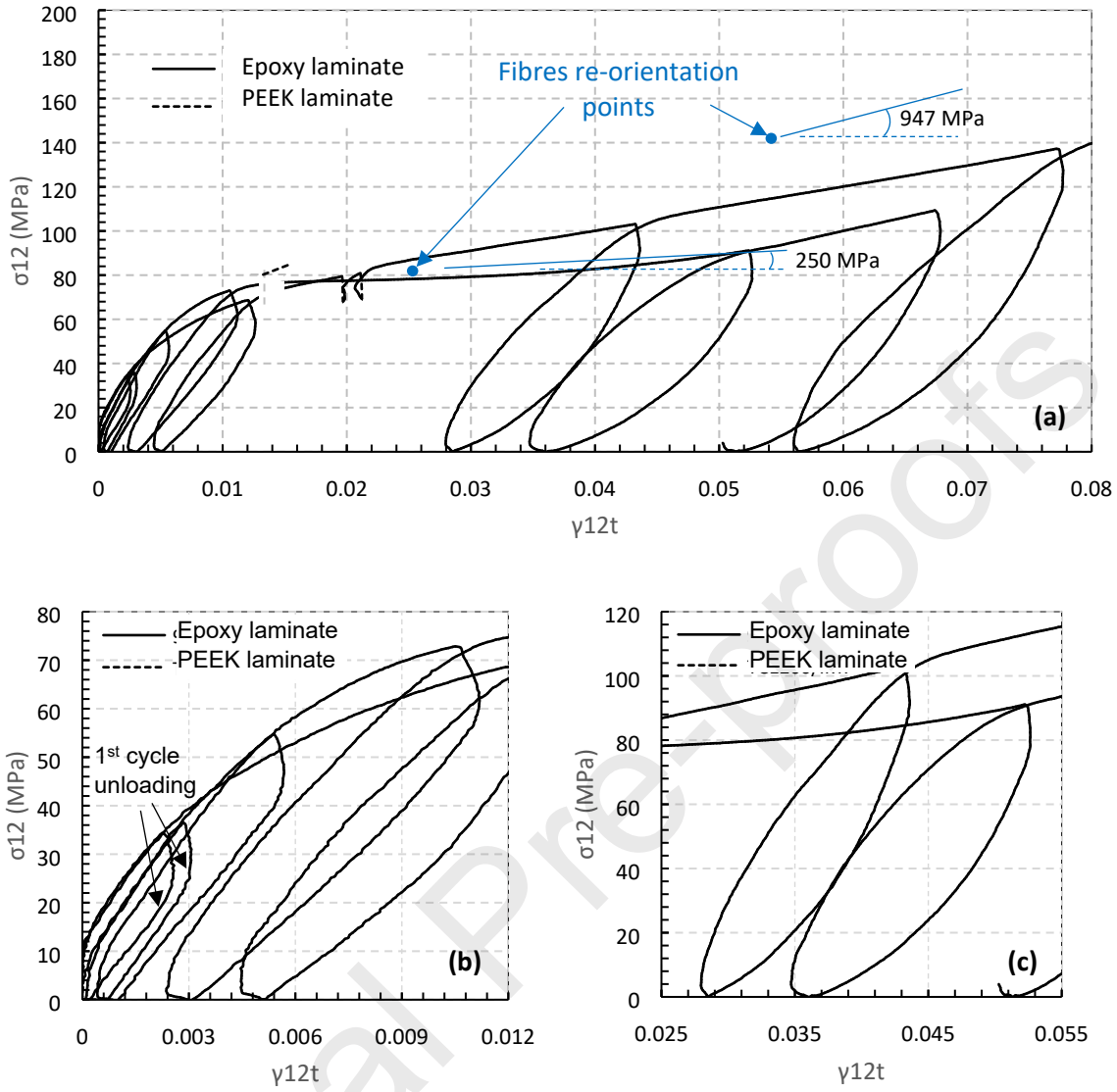

Figure 4. Stress-strain data for (a) ±45° TS laminates 977-6/T800 (solid line) and TP laminate TC1200/IM7 (dashed line), (b) data for γ_{12}= 0 – 0.012, (c) data for γ_{12}= 0.025 – 0.055

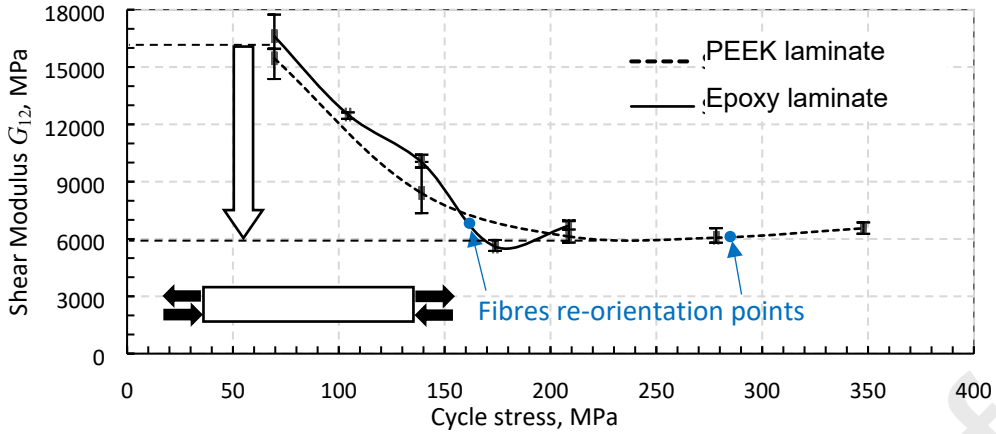

Figure 5. Shear modulus evolution versus applied stress ($2\sigma_{12}$; values in Table 1) for (±45°) tensile cyclic testing 977-6/T800 (solid line) and TC1200/IM7 (dashed line); The re-orientation points have been transferred from the blue points identified in Figure 4(a).

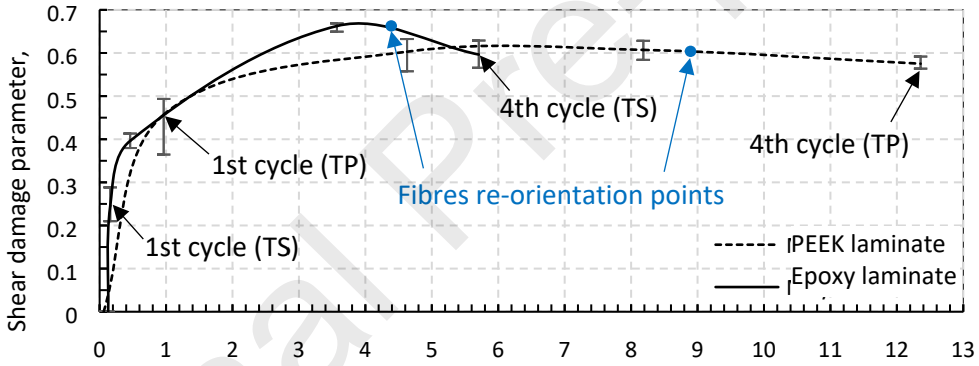

Figure 6. Shear damage parameter (d_{12}) evolution during ±45° tensile cyclic testing of 977-6/T800 (solid line) and TC1200/IM7 (dashed line); The re-orientation points have been transferred from the blue points identified in Figure 4(a).

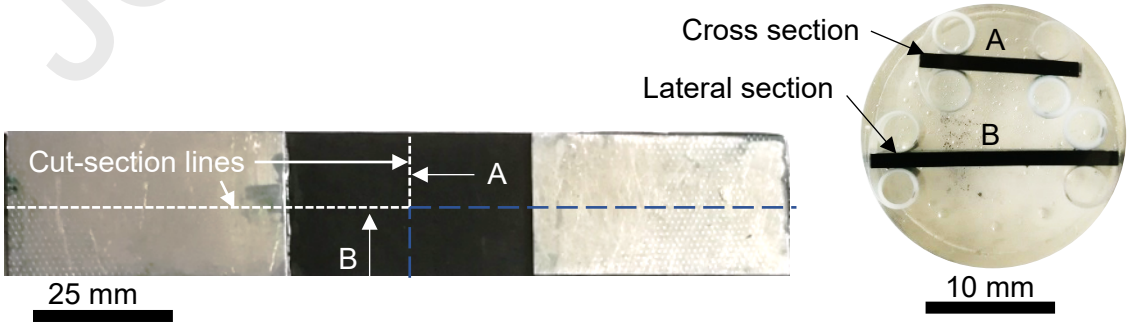

Figure 7. Lateral and cross sectional cut lines for microscopic investigations

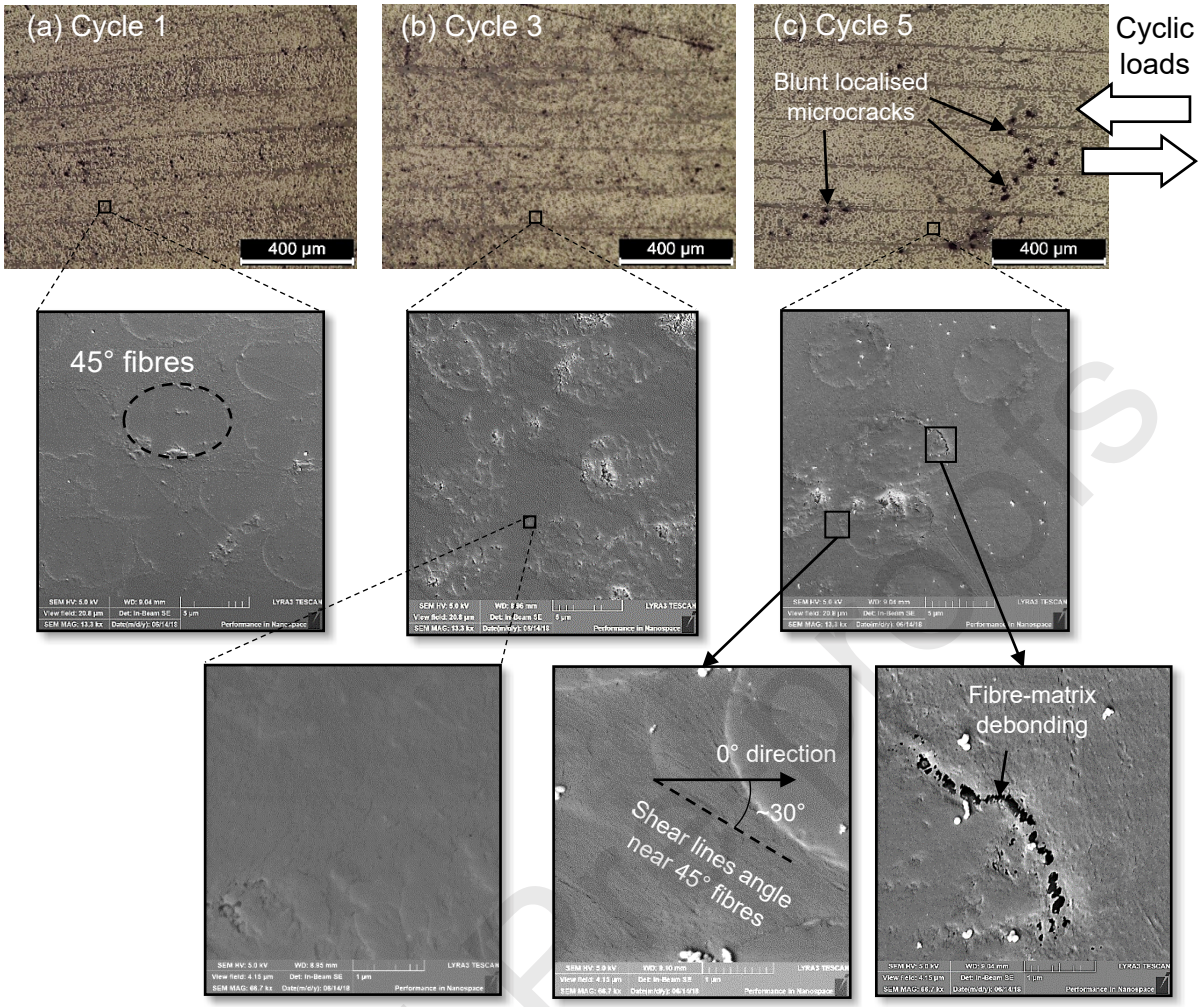

Figure 8. Microscopic observations of PEEK laminates at (a) Cycle 1 (γ_{12}= 0.24%), (b) Cycle 3 (γ_{12}= 4.3%), and (c) Cycle 5 (γ_{12}= 10.8%)

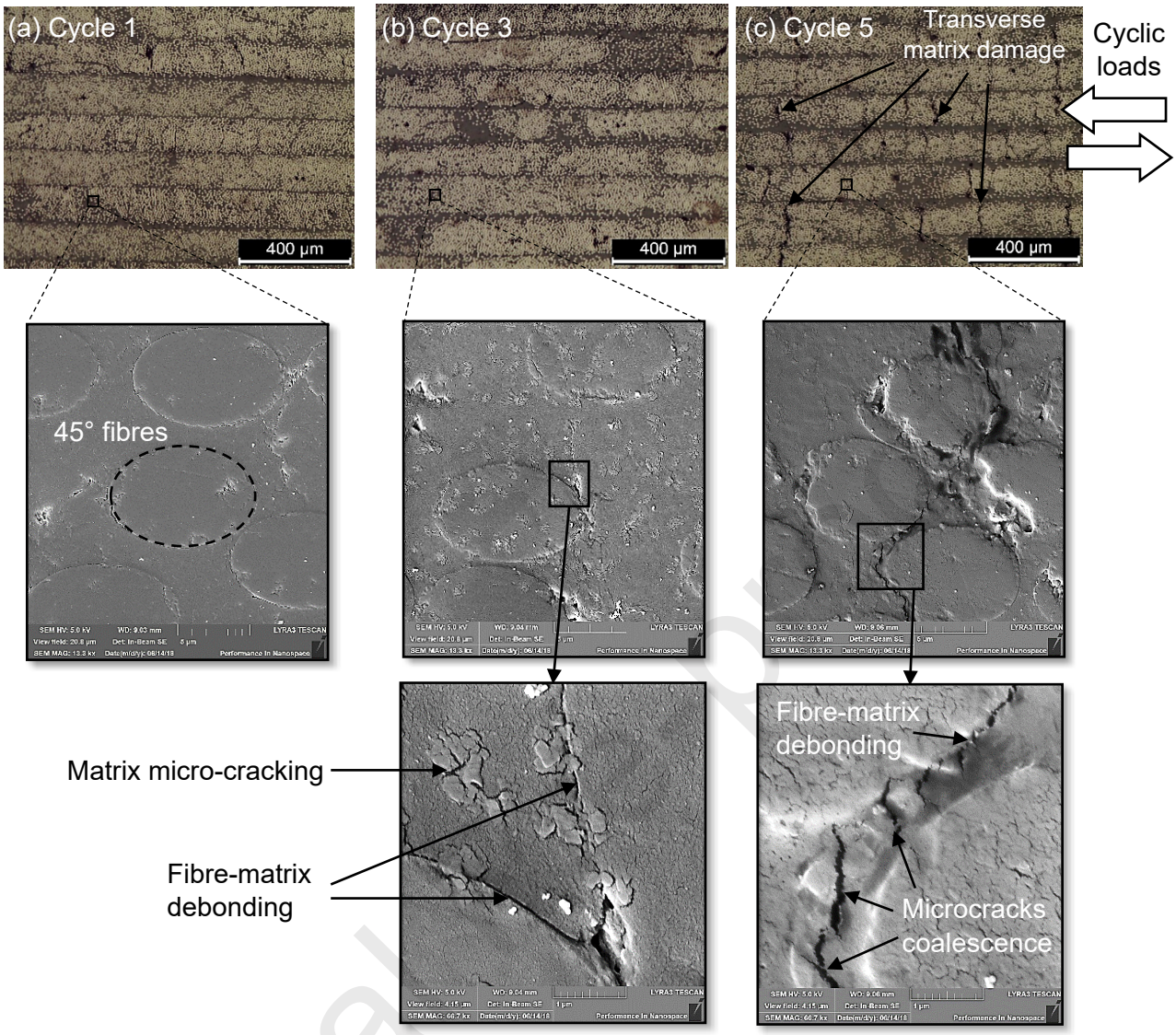

Figure 9. Microscopic observations of Epoxy laminates at (a) Cycle 1 (γ_{12}= 0.3%), (b) Cycle 3 (γ_{12}= 1.1%), and (c) Cycle 5 (γ_{12}= 6.7%)

Authors Statement:

Submission ID: COST_2020_1998

Revised Title: Shear Driven Deformation and Damage Mechanisms in High-performance Carbon Fibre-reinforced Thermoplastic and Toughened Thermoset Composites Subjected to High Strain Loading

A. Mills and H.Y. Nezhad have supervised the research conducted by T.P. Hernandez as a funded doctoral research. T.P. Hernandez carried out the experimental research, and together with H.Y. Nezhad utilised continuum damage mechanics' expressions for

calculation of damage parameters. A. Mills, T.P. Hernandez and H.Y. Nezhad were together involved in critical thinking and analysis of the results. T.P. Hernandez provided the first draft of the article which was further revised by H.Y. Nezhad and A. Mills.